Acta Crystallographica Section D
Biological Crystallography
ISSN 1399-0047

The structure of a novel electron-transfer ferredoxin from *Rhodopseudomonas palustris* HaA2 which contains a histidine residue in its iron–sulfur cluster-binding motif

Ting Zhang,[a] Aili Zhang,[a] Stephen G. Bell,[b,c]* Luet-Lok Wong[c] and Weihong Zhou[a]*

[a]College of Life Sciences, Nankai University, Tianjin 300071, People's Republic of China, [b]School of Chemistry and Physics, University of Adelaide, Adelaide, SA 5005, Australia, and [c]Department of Chemistry, University of Oxford, Inorganic Chemistry Laboratory, South Parks Road, Oxford OX1 3QR, England

Correspondence e-mail: stephen.bell@adelaide.edu.au, weihong.zhou@gmail.com

Received 13 January 2014
Accepted 1 March 2014

PDB references: HaPuxC, 4id8; 4ov1

Rhodopseudomonas palustris HaA2 contains a gene, *RPB3630*, encoding a ferredoxin, HaPuxC, with an atypical C*XX*H*XX*C(*X*)$_n$CP iron–sulfur cluster-binding motif. The ferredoxin gene is associated with a cytochrome P450 (CYP) monooxygenase-encoding gene, CYP194A3, an arrangement which is conserved in several strains of bacteria. Similar ferredoxin genes are found in other bacteria, such as *Mycobacterium tuberculosis*, where they are also associated with CYP genes. The crystal structure of HaPuxC has been solved at 2.3 Å resolution. The overall fold of this [3Fe–4S] cluster-containing ferredoxin is similar to other [3Fe–4S] and [4Fe–4S] species, with the loop around the iron–sulfur cluster more closely resembling those of [3Fe–4S] ferredoxins. The side chain of His17 from the cluster-binding motif in HaPuxC points away from the vacant site of the cluster and interacts with Glu61 and one of the sulfide ions of the cluster. This is the first cytochrome P450 electron-transfer partner of this type to be structurally characterized and will provide a better understanding of the electron-transfer processes between these ferredoxins and their CYP enzymes.

1. Introduction

Iron–sulfur clusters are functionally versatile and ancient prosthetic groups that are widespread in nature and are involved in processes critical to life (Johnson *et al.*, 2005; Meyer, 2008). One of the primary roles of iron–sulfur cluster ferredoxins is in mediating biological electron transfer, and they are well suited to this task by virtue of their ability to delocalize electron density over the Fe and S atoms of the cluster (Johnson *et al.*, 2005; Cordes & Giese, 2009). Ferredoxins are commonly found as the electron-transfer partners of cytochrome P450 enzymes (CYP; Hannemann *et al.*, 2007).

The haem-dependent CYP enzymes catalyze the insertion of an O atom from atmospheric dioxygen into carbon–hydrogen bonds. The enzymatic activity of CYP enzymes requires two electrons that are usually derived from NAD(P)H and delivered to the P450s by their electron-transfer partners. Bacterial CYP enzymes generally use class I electron-transfer chains that consist of an oxygenase-coupled NAD(P)H-dependent ferredoxin reductase (ONFR) and an iron–sulfur ferredoxin. The ONFR typically contains a FAD cofactor, and ferredoxin cluster types include [2Fe–2S], [3Fe–4S], [4Fe–4S] and combinations of these (Chun *et al.*, 2007; Green *et al.*, 2003; Hannemann *et al.*, 2007; Mandai *et al.*, 2009; Munro *et al.*, 2007). As the number of available genome

sequences has grown, the array of CYP enzymes and their electron-transfer partners has expanded and diversified to include fusion proteins and flavodoxins (Bell *et al.*, 2013; Hawkes *et al.*, 2002; Whitehouse *et al.*, 2012; Jackson *et al.*, 2002, 2007; Roberts *et al.*, 2002). Bacterial CYP enzymes often show redox-partner specificity and electron transfer is tightly regulated (Brazeau *et al.*, 2003; Xu *et al.*, 2009; Yang *et al.*, 2010; Sevrioukova & Poulos, 2011) and, while they can be produced heterologously, it is difficult to identify competent electron-transfer partner proteins to reconstitute the monooxygenase activity. This hampers efforts to understand their physiological function and their downstream utilization as C—H bond oxidation catalysts in biotechnological applications.

Rhodopseudomonas palustris is a member of a family of purple photosynthetic bacteria that have been isolated from diverse environments. They possess extraordinary metabolic versatility and can grow under anaerobic or aerobic conditions with or without light, can fix nitrogen and have a wide range of biodegradation capabilities (Larimer *et al.*, 2004). Studies have shown that different *Rhodopseudomonas* species share many characteristics but each has a unique set of functional genes to take advantage of the environment in which they are found (Oda *et al.*, 2002, 2004, 2008). We have reported the properties of several of the seven CYP enzymes found in *R. palustris* strain CGA009 and have found that they are capable of binding a range of substituted benzenes, phenols, benzaldehydes and benzoic acids (Bell *et al.*, 2006).

The complete CYP199A2 and CYP199A4 class I P450 systems from *R. palustris* strains CGA009 and HaA2 have been isolated and studied (Bell, Tan *et al.*, 2010; Xu *et al.*, 2009; Bell *et al.*, 2008; Bell, Zhou *et al.*, 2012). Both are class I electron-transfer chains consisting of a [2Fe–2S] ferredoxin (Pux and HaPux) and a FAD-dependent ferredoxin reductase (PuR and HaPuR) (Bell *et al.*, 2006; Bell, Tan *et al.*, 2010; Bell, Xu *et al.*, 2010; Xu *et al.*, 2009). CYP199A2 and CYP199A4 both catalyse the oxidative demethylation of 4-methoxybenzoic acid and the hydroxylation and desaturation of 4-ethylbenzoic acid with high activity (Bell *et al.*, 2006, 2008; Bell, Tan *et al.*, 2010; Bell, Zhou *et al.*, 2012). The PuR/Pux and HaPuR/HaPux electron-transfer proteins can support the CYP199 family enzyme from the other system, but are not able to efficiently support the monooxygenase function of the additional CYP enzymes from either *R. palustris* strain. *R. palustris* CGA009 contains a second [2Fe–2S] ferredoxin, PuxB, which shares high sequence identity with iron–sulfur cluster biogenic ferredoxins. This ferredoxin was also unable to reconstitute the activity of the other CYP enzymes from *R. palustris*, although it showed moderate activity with CYP199A2 (Bell, McMillan *et al.*, 2012; Bell, Xu *et al.*, 2010).

A third ferredoxin gene (*RPA1731* and *RPB3630*) is present in the genomes of both *R. palustris* CGA009 and HaA2 and is associated with a CYP194A family gene (*RPA1730* and *RPB3631*, respectively) (Bell *et al.*, 2006). Here, we report the isolation, production and crystal structure of the ferredoxin HaPuxC encoded by the *RPB3630* gene of *R. palustris* HaA2. This ferredoxin has a histidine residue in the iron–sulfur cluster-binding motif.

2. Materials and methods

2.1. General

General DNA and microbiological experiments were carried out using standard methods (Sambrook *et al.*, 1989). The KOD polymerase used for the PCR steps and the pET-26a expression vector were from Merck Biosciences, UK and other enzymes for molecular biology were from New England Biolabs, UK. General reagents were from Sigma–Aldrich or Merck, UK. Isopropyl β-D-1-thiogalactopyranoside (IPTG), growth media and buffer components were from Melford Laboratories, UK and NADH was from Roche Diagnostics, UK, Invitrogen, USA or the Beijing Chemical Company, People's Republic of China. Plates for use in crystallography were from Tianjin Xiangyushun Macromolecule Technology Ltd, People's Republic of China. All sequence alignments were performed using *Clustal* and were analysed using *ESPript* (http://espript.ibcp.fr; Chenna *et al.*, 2003; Gouet *et al.*, 2003) or *Phylodendron* (http://iubio.bio.indiana.edu/treeapp/treeprint-form.html).

2.2. Cloning, expression and purification

The gene encoding the the putative [3Fe–4S] ferredoxin HaPuxC from *R. palustris* HaA2 was amplified by PCR using the following oligonucleotide primers (the restriction sites are highlighted in bold with stop codons in italics): HaPuxC 5′, 5′-ttaatt**catatg**tccgaaatgctgaccatc-3′; HaPuxC 3′, 5′-taaatt**aagctt*tta***gtcttctgtgatgtcgatcgc-3′. The gene was amplified by 25 cycles of strand separation at 95°C for 1 min followed by annealing at 50°C and extension at 68°C for 40 s. The PCR amplification of the [3Fe–4S] ferredoxin gene *RPB1731* from *R. palustris* CGA009 has been reported previously (Bell *et al.*, 2006). The genes encoding the ferredoxins were cloned into the expression vector pET-26b using the *Nde*I and *Hin*dIII restriction sites.

The recombinant plasmids were transformed into *Escherichia coli* strain BL21 (DE3) for protein production. The transformed bacterial cells were cultured in 2×YT medium supplemented with trace elements and 25 µg ml^{-1} kanamycin at 37°C. When the OD_{600} of the culture reached 0.6–0.8, 0.15 m*M* IPTG was added in order to induce production of the recombinant protein. After further growth for 24 h at 20°C, the cells were harvested by centrifugation.

The cell pellets were resuspended in buffer *P* (10 m*M* Tris pH 7.4, 10% glycerol, 1 m*M* DTT) and the cells were lysed by sonication at 4°C. The crude extracts were then centrifuged at 27 000*g* for 45 min at 4°C to remove cell debris. The brown supernatant containing the protein was injected onto a Fast Flow Sepharose Q column (GE Healthcare, USA) and eluted with a gradient of 0–1 *M* NaCl in buffer *P*. The ferredoxin was collected (elution at ∼290 m*M* NaCl), concentrated by ultrafiltration to 1 ml and then buffer-exchanged into buffer *A* (20 m*M* Tris pH 7.4, 1 m*M* DTT). The protein solution in buffer *A* was concentrated to 1 ml, injected onto a HiTrap Q column (GE Healthcare, USA) and eluted with a gradient of 0–1 *M* NaCl in buffer *A*. The brown protein which eluted at ∼280 m*M* NaCl was collected, concentrated by ultrafiltration

to 500 µl, applied onto a Superdex 75 gel-filtration chromatography column (GE Healthcare, USA) and eluted with buffer *A* containing 150 m*M* NaCl. The purity of the protein was checked by SDS–PAGE (Supplementary Fig. S1[1]). The protein was stored at −20°C in 50 m*M* Tris pH 7.4 containing 50%(*v*/*v*) glycerol.

2.3. Protein assays

Glycerol was removed immediately before use by gel filtration on a 5 ml PD-10 column (GE Healthcare, UK) using 50 m*M* Tris pH 7.4. UV–Vis spectroscopic assays were recorded at 30 ± 0.5°C on a Varian Cary 50 or Cary 1E spectrophotometer. Reduction of the ferredoxin was carried out in a sealed cuvette (1.5 ml) containing 50 m*M* Tris pH 7.4, 30 µ*M* ferredoxin and 0.5 µ*M* HaPuR. An excess of NADH (∼20 µ*M*) was added to reduce the protein.

2.4. Crystallization

The ferredoxin was concentrated to 50 mg ml^{-1} in buffer *A* containing 150 m*M* NaCl. The sitting-drop vapour-diffusion method was used with Crystal Screen, Crystal Screen 2 and Index (Hampton Research, USA) to grow crystals of the ferredoxin at 16°C in 48-well plates. Two drops (each of 1 µl) of the protein solution at 15 or 25 mg ml^{-1} protein were mixed with 1 µl reservoir solution and equilibrated against 100 µl reservoir solution. After about a week, several tawny needle-like crystals were obtained from Crystal Screen 2 condition No. 14 (0.2 *M* potassium sodium tartrate tetrahydrate, 0.1 *M* sodium citrate tribasic dihydrate pH 5.6, 2.0 *M* ammonium sulfate) and Crystal Screen condition No. 32 (2.0 *M* ammonium sulfate).

The crystallization conditions were further optimized by changing the concentration of precipitants and protein, the buffer pH value and the temperature using condition No. 14 from Crystal Screen 2 as a starting point. The crystals were grown by vapour diffusion in hanging drops at 16°C in 24-well plates and equilibrated against 300 µl reservoir solution. Many thin rod-like crystal clusters were obtained which were not suitable for data collection. The micro-seeding method was used to improve the quality of the crystals. The thin rod-like crystal clusters were exchanged into 2 µl fresh reservoir solution and then mashed with a needle. This mixture was added to 50 µl fresh reservoir solution containing a bead as a seeding stock. The bead and seeding stock were fully blended using a magnetic stirrer. The seeding stock was then diluted fivefold, 25-fold, 125-fold and 500-fold and crystals were grown using the hanging-drop vapour-diffusion method. Thick rod-like crystals which yielded the best diffraction data were obtained using the conditions 0.3 *M* potassium sodium tartrate tetrahydrate, 0.1 *M* Tris pH 8.5, 2.4 *M* ammonium sulfate using a seed stock of fivefold dilution and a protein concentration of 15 mg ml^{-1}.

[1] Supporting information has been deposited in the IUCr electronic archive (Reference: MN5055).

Table 1
Data-collection and refinement statistics of the [3Fe–4S] ferredoxin HaPuxC from *R. palustris* HaA2.

Data-collection statistics	
Space group	$P2_12_12_1$
Unit-cell parameters (Å)	a = 23.4, b = 26.8, c = 91.2
Wavelength (Å)	1.5418
Resolution† (Å)	50–2.30 (2.35–2.30)
Average $I/\sigma(I)$†	19.3 (12.3)
Completeness† (%)	96.4 (80.8)
Average multiplicity†	4.7 (3.3)
$R_{\rm merge}$†‡ (%)	7.4 (12.6)
Molecules in asymmetric unit	1
Structure-refinement statistics	
Resolution (Å)	23.11–2.31
Average B factor (Å^2)	24.5
$R_{\rm cryst}/R_{\rm free}$§ (%)	22.3/24.5
R.m.s.d., bond lengths (Å)	0.014
R.m.s.d., bond angles (°)	1.503
No. of unique reflections used for refinement	2671
Total No. of atoms (protein, [3Fe–4S], H_2O *etc.*)	523 (13 water molecules, 1 [3Fe–4S] cluster)
Ramachandran favoured (%)	98.44
Ramachandran outliers (%)	1.56
MolProbity score	1. 57
Poor rotamers (%)	0
Clashscore, all atoms	11.24

† Values in parentheses are for the highest resolution shell. ‡ $R_{\rm merge} = \sum_{hkl}\sum_i |I_i(hkl) - \langle I(hkl)\rangle| / \sum_{hkl}\sum_i I_i(hkl)$, where $I_i(hkl)$ is the ith intensity measurement of reflection hkl and $\langle I(hkl)\rangle$ is the average intensity from multiple observations. § $R_{\rm cryst}/R_{\rm free} = \sum_{hkl} \big||F_{\rm obs}| - |F_{\rm calc}|\big| / \sum_{hkl} |F_{\rm obs}|$, where $F_{\rm obs}$ and $F_{\rm calc}$ are the observed and calculated structure factors, respectively.

2.5. Crystallographic data collection and processing

X-ray diffraction data were collected on a Rigaku MicroMax-007 rotating-anode X-ray generator operating at 40 kV and 30 mA. Crystals were flash-cooled at −173°C in a nitrogen-gas stream after cryoprotection with 25% glycerol in the reservoir solution. The diffraction data were collected to 2.15 Å resolution. The intensity set was indexed, integrated and scaled with the *HKL*-2000 package (Otwinowski & Minor, 2001). Molecular replacement was carried out with *Phaser* in the *CCP*4 suite (McCoy *et al.*, 2007). The crystals belonged to space group $P2_12_12_1$, with unit-cell parameters a = 23.4, b = 26.8, c = 91.1 Å and one molecule in the asymmetric unit. Complete data-collection statistics and results are summarized in Table 1.

2.6. Structure determination and refinement

The phases were found using the *Phaser* molecular-replacement method in the *CCP*4 suite (McCoy *et al.*, 2007). The structure of the D14C mutant of the [4Fe–4S] ferredoxin from *Pyrococcus furiosus* (PDB entry 2z8q; Løvgreen *et al.*, 2011) was used as a search model. The model was rebuilt with *Coot* (Emsley & Cowtan, 2004) and refined with *phenix.refine* (Adams *et al.*, 2010). The default restraints were used in the refinement. The final structure was obtained by TLS refinement with parameters generated by the *TLSMD* web server (Painter & Merritt, 2006*a*,*b*). The stereochemical quality of the refined structure was checked with *MolProbity* (Chen *et al.*, 2010). A summary of the structure-refinement statistics is provided in Table 1. The coordinates of the crystal structure

has been deposited in the PDB (http://www.pdb.org) with accession code 4ov1.

2.7. Protein structure modeling

The automated protein structure homology-modelling server *SWISS-MODEL* (http://swissmodel.expasy.org/) was used to model the structure of the [3Fe–4S] ferredoxin from *Mycobacterium tuberculosis* (the product of gene *Rv0763c*; Arnold *et al.*, 2006; Kiefer *et al.*, 2009; Peitsch, 1995; McLean *et al.*, 2006). The crystal structure of the [3Fe–4S] ferredoxin from the hyperthermophilic archaeon *P. furiosus* (PDB entry 1siz; Nielsen *et al.*, 2004) was used as the model structure and the resulting modelled structure was used without any further modification.

3. Results

3.1. HaPuxC purification and properties

A third potential ferredoxin gene was identified in the genomes of both *R. palustris* strains CGA009 (*RPA1731*) and HaA2 (*RPB3630*). In both instances the ferredoxin gene is found next to a CYP-encoding gene (*RPA1730* in CGA009 and *RPB3631* in HaA2), both of which encode a CYP194A enzyme. As such, the encoded ferredoxin proteins would be expected to function as electron-transfer partners for the CYP194 enzymes. The ferredoxin genes were readily amplified *via* PCR and cloned into the pET-26a expression vector. The determined nucleotide sequences of the cloned genes were in complete agreement with those in the genome database. We have previously identified and characterized two ferredoxins from *R. palustris* strain CGA009 (Pux and PuxB), both of which have equivalent genes in the HaA2 strain of *R. palustris* (Bell, McMillan *et al.*, 2012; Bell, Tan *et al.*, 2010; Bell & Wong, 2007; Bell, Xu *et al.*, 2010). We therefore named the two new ferredoxins from the CGA009 and HaA2 strains of *R. palustris* PuxC and HaPuxC.

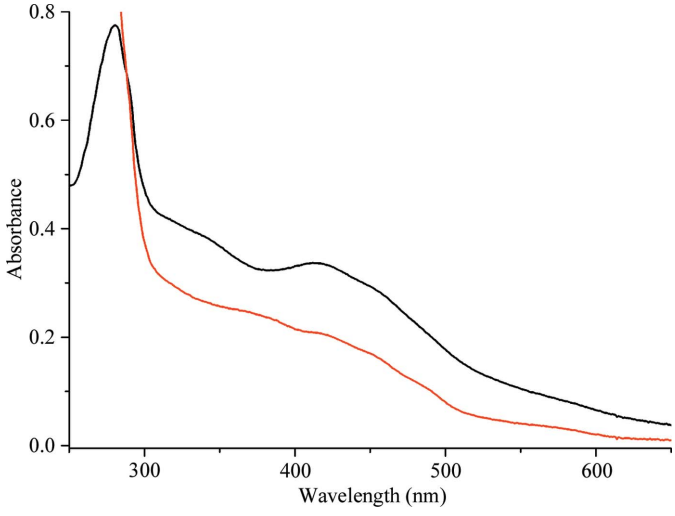

Figure 1
The UV–Vis spectra of the [3Fe–4S] ferredoxin HaPuxC from *R. palustris* HaA2: black, as purified; red, after reduction with HaPuR and NADH.

Both ferredoxins (HaPuxC and PuxC) were produced in a soluble form using *E. coli* (Supplementary Fig. S1). The purified ferredoxins were brown in colour and showed very similar spectral properties to those reported for other [3Fe–4S] and [4Fe–4S] cluster-containing ferredoxins (Duderstadt *et al.*, 1999; McLean *et al.*, 2006). Their spectra were comparable with that reported for the histidine-containing ferredoxin from *M. tuberculosis*, with maxima at 283 and 412 nm and broad shoulders at 330, 460 and 580 nm (Fig. 1; McLean *et al.*, 2006). HaPuxC was produced in greater amounts and yielded crystals more readily than PuxC, and we chose to focus on this ferredoxin for further study (the ferredoxins share 85% sequence identity). Reduction of HaPuxC using NADH mediated *via* a ferredoxin reductase from *R. palustris* strains HaA2 or CGA009 (HaPuR or PuR, respectively; Bell, Tan *et al.*, 2010; Xu *et al.*, 2009) resulted in a reduction in the intensity of the absorption spectrum above 300 nm (Fig. 1).

The two CYP194A enzymes were classified using the standard nomenclature (CYP194A2 and CYP194A3; see Supporting Information) and could be produced in a soluble form in *E. coli* (Nelson *et al.*, 1996). Unusually, both were isolated in the high-spin ferric form with Soret maxima at 390 nm, although both showed the characteristic 447 nm absorption for the iron(II)(CO) complex (data not shown). Neither P450 enzyme could be induced to convert to low spin by size-exclusion chromatography before or after reduction, temperature or pH changes, or by the addition of alcohols or other substrates (Sineva & Davydov, 2010; McLean *et al.*, 2009). This prevented detailed substrate-binding studies and complicates the investigation of electron transfer from the ferredoxins to these CYP194A family enzymes. Further studies are required to ascertain whether this is the resting state of the CYP194A enzymes and what effect it might have on their electron-transfer properties. Other CYP enzymes and mutant CYPs have been isolated as a mixture of spin states (Warrilow *et al.*, 2009; Sineva & Davydov, 2010; Whitehouse *et al.*, 2009; Xu *et al.*, 2005; Capyk *et al.*, 2009).

3.2. Comparison of HaPuxC with other ferredoxins

Both the PuxC and HaPuxC ferredoxins from *R. palustris* strains CGA009 and HaA2 have sequence similarities to [3Fe–4S] and [4Fe–4S] ferredoxins from a diverse range of bacteria (Bell *et al.*, 2006; Fukuyama *et al.*, 1989; Green *et al.*, 2003; Kissinger *et al.*, 1991; Løvgreen *et al.*, 2011; Nielsen *et al.*, 2004). These ferredoxins all have the **C***XXXXXX***C**$(X)_n$**CP** motif with the three cysteine-residue side chains acting as ligands to three of the irons in the cluster (Fig. 2). The residue corresponding to ***X*** varies among the ferredoxin proteins. In the [4Fe–4S] ferredoxins ***X*** is normally a cysteine residue which acts as a ligand to the fourth iron in the cluster. A **C***XX***A**/**G***XX***C**$(X)_n$**CP** motif, where ***X*** is A or G, is usually found in [3Fe–4S] cluster ferredoxins. In HaPuxC a histidine residue (His17) replaces the second cysteine in the [4Fe–4S] ferredoxin motif or the glycine or alanine residue in the [3Fe–4S] ferredoxin motif [**C***XX***HXXC**$(X)_n$**CP**].

Stucturally characterized [3Fe–4S] and [4Fe–4S] iron–sulfur cluster ferredoxins have been reported previously. These include those from *Desulfovibrio gigas*, *P. furiosus*, *Thermotoga maritima* and *Bacillus thermoproteolyticus* (see below). The latter two ferredoxins are [4Fe–4S] clusters (***X*** = C). The ferredoxin from the sulfate-reducing bacterium *D. gigas* (***X*** = C) exists in two oligomeric forms. The first is a dimer in which each of the subunits contains a single [4Fe–4S] cluster, while the other is a tetramer in which the clusters are of the [3Fe–4S] variety. These two forms can interconvert reversibly (Kissinger *et al.*, 1991). In the ferredoxin from *P. furiosus* the ***X*** residue is an aspartate (Asp14). This ferredoxin contains a [4Fe–4S] cluster when isolated under anaerobic conditions, but a [3Fe–4S] cluster when oxidized (Duderstadt *et al.*, 1999; Nielsen *et al.*, 2004; Zhou & Adams, 1997). Mutation of this aspartate residue to a cysteine retains and stabilizes the [4Fe–4S] cluster. Mutation to serine also maintains the [4Fe–4S] cluster, while mutation to valine, histidine, tyrosine or asparagine yields a [3Fe–4S] cluster (Duderstadt *et al.*, 1999).

The best characterized [3Fe–4S] CYP enzyme electron-transfer carriers are those which have the **C***XX***A**/**G***XX*-**C**(*X*)$_n$**CP** [3Fe–4S] motif from *Streptomyces* species (Chun *et al.*, 2007; Lamb *et al.*, 2002; Chiu *et al.*, 2001). We and others have identified several other bacterial ferredoxins that are associated with CYP enzymes that have the **C***XX***H***XX*-**C**(*X*)$_n$**CP** motif, in which a histidine replaces the glycine or alanine residue. These include ferredoxins from different *Mycobacterium* strains, including *M. tuberculosis* (McLean *et al.*, 2006; Jackson *et al.*, 2002; Poupin *et al.*, 1999; Sielaff & Andreesen, 2005; Sielaff *et al.*, 2001). In addition to the HaPuxC and PuxC ferredoxins, we observe that similar ferredoxin-encoding genes are found in *R. palustris* strain BisB5 (*RPD1837*), *Bradyrhizobium japonicum* USDA110 (*bsl2906*) and *Novosphingobium aromaticivorans* (*saro_3681*), and all of these are associated with CYP enzymes (Oda *et al.*, 2008; Bell *et al.*, 2006; Bell & Wong, 2007; Kaneko *et al.*, 2002).

Analysis of the amino-acid sequences of these species showed that the histidine-containing ferredoxins cluster together with the *Streptomyces* [3Fe–4S] ferredoxins and the [4Fe–4S] ferredoxin from *Clostridium thermoaceticum* (Fig. 2*b*; Elliott *et al.*, 1982). The ferredoxins from the *R. palustris* strains and *N. aromaticivorans* cluster together, while the *Mycobacterium* ferredoxins are more closely related to the alanine/glycine-containing [3Fe–4S] ferredoxins from *Streptomyces* species (Fig. 2*b*). The [4Fe–4S] ferredoxins from *P. furiosus*, *T. maritima* and *D. gigas* cluster together as a group, as do those of the *Bacillus* strains. Overall, the alignments suggest that these histidine-containing proteins are more closely related to the [3Fe–4S] ferredoxins from *Streptomyces* strains than to the [4Fe–4S] ferredoxins (Fig. 2*b*).

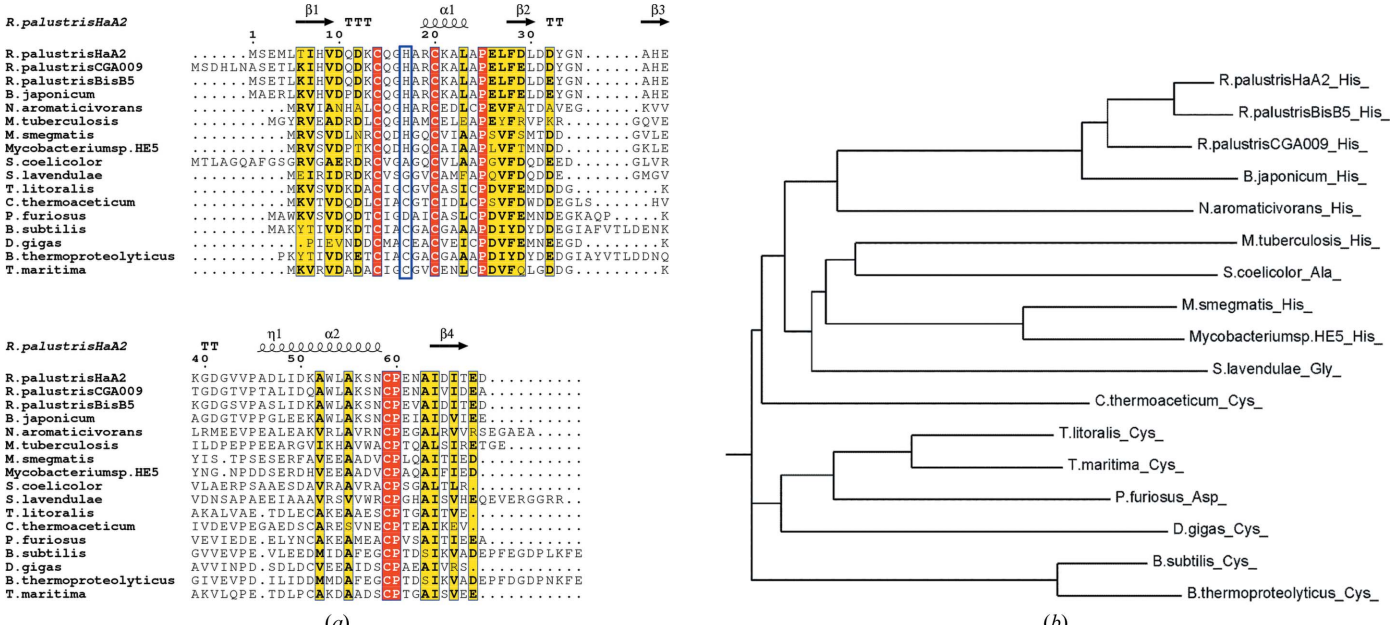

(*a*) (*b*)

Figure 2
(*a*) Structural sequence alignment of the [3Fe–4S] ferredoxin HaPuxC from *R. palustris* HaA2 with other [3Fe–4S] and [4Fe–4S] ferredoxins, including the structurally characterized ferredoxins from *Desulfovibrio gigas* (PDB entry 1fxd), *Bacillus thermoproteolyticus* (PDB entry 1iqz), *Thermotoga maritima* (PDB entry 1vjw) and the aspartate-containing ferredoxin from *Pyrococcus furiosus* (PDB entry 1sj1). Other ferredoxins include the [3Fe–4S] ferredoxins from *Streptomyces coelicolor* and *S. lavendulae*, the [4Fe–4S] ferredoxins from *Thermococcus litoralis*, *B. subtilis* and *Clostridium thermoaceticum*, and ferredoxins with histidine in the iron–sulfur cluster-binding motif from *Mycobacterium tuberculosis*, *M. smegmatis*, *Mycobacterium* species HE5, *R. palustris* CG009, *R. palustris* BisB5, *Novosphingobium aromaticivorans* and *Bradyrhizobium japonicum* USDA 110. Conserved residues, including the cysteine residues of the ferredoxin motif, are shaded in red. The variable residue ***X*** of the **C***XXXXX***C**(*X*)$_n$**CP** motif is highlighted inside a blue box. β-Sheet A consists of β1 and β4; β-sheet B consists of β2 and β3. The intitial methionine residue of the ferredoxins from *P. furiosus* and *T. maritima* are included as per the sequence of their crystal structures in the PDB. We have included the methionine start codon of RPB3630 from *R. palustris* HaA2. (*b*) A phylogenenetic tree of the protein sequence of the [3Fe–4S] and [4Fe–4S] ferredoxins aligned in (*a*). The branches of the tree have been labelled with the name of the bacterium of origin of the ferredoxin and the amino-acid residue that occupies position ***X*** of the **C***XXXXX***C**(*X*)$_n$**CP** motif. The phenogram was generated by *Phylodendron* using the default parameters (http://iubio.bio.indiana.edu/treeapp/treeprint-form.html).

3.3. Overall structure of *R. palustris* HaA2 ferredoxin

The crystals of HaPuxC from *R. palustris* HaA2 belonged to space group $P2_12_12_1$ and there is only one molecule in the asymmetric unit. The polypeptide chain can be traced from Leu5 to Asp69. The structure conforms to that expected for a ferredoxin containing a single [3Fe–4S] or [4Fe–4S] cluster (Fig. 3; Macedo-Ribeiro *et al.*, 1996; Kissinger *et al.*, 1991). There are two α-helices, a short α-helix 1 (Arg19–Leu23) and a longer α-helix 2 (Ile49–Asn58), and two antiparallel β-sheets, β-sheet A (Thr6–Val9 and Ile64–Thr67) and β-sheet B (Phe28–Asp31 and Gly34–Glu38). These helices and sheets are connected by five turns (A–E). The electron density of the iron–sulfur cluster clearly identifies it as a [3Fe–4S] cluster. 98.4% of the residues are in the favoured region of the Ramachandran plot.

The structure of HaPuxC was compared with structurally characterized ferredoxins (Fig. 3), including those containing a [3Fe–4S] cluster from *D. gigas* (PDB entry 1fxd; Kissinger *et al.*, 1991) and *P. furiosus* (PDB entry 1sj1; Nielsen *et al.*, 2004) and those with a [4Fe–4S] cluster from *T. maritima* (PDB entry 1vjw; Macedo-Ribeiro *et al.*, 1996), *B. thermoproteolyticus* (PDB entry 1iqz; Fukuyama *et al.*, 1989) and *P. furiosus* (a mutant form of the enzyme containing the mutation D14C; PDB entry 2z8q; Løvgreen *et al.*, 2011). The ferredoxins have very similar structures: all share the two α-helices and two double-strand β-sheets (Fig. 3). However, there are differences; β-sheet B (β2 and β3) of the [3Fe–4S] ferredoxin HaPuxC from *R. palustris* HaA2 is longer than those in all of the other ferredoxins (Supplementary Fig. S2). There is also a longer turn D between β-sheet B and α-helix 2 compared with the ferredoxins from *D. gigas* and *T. maritima*, but this turn is

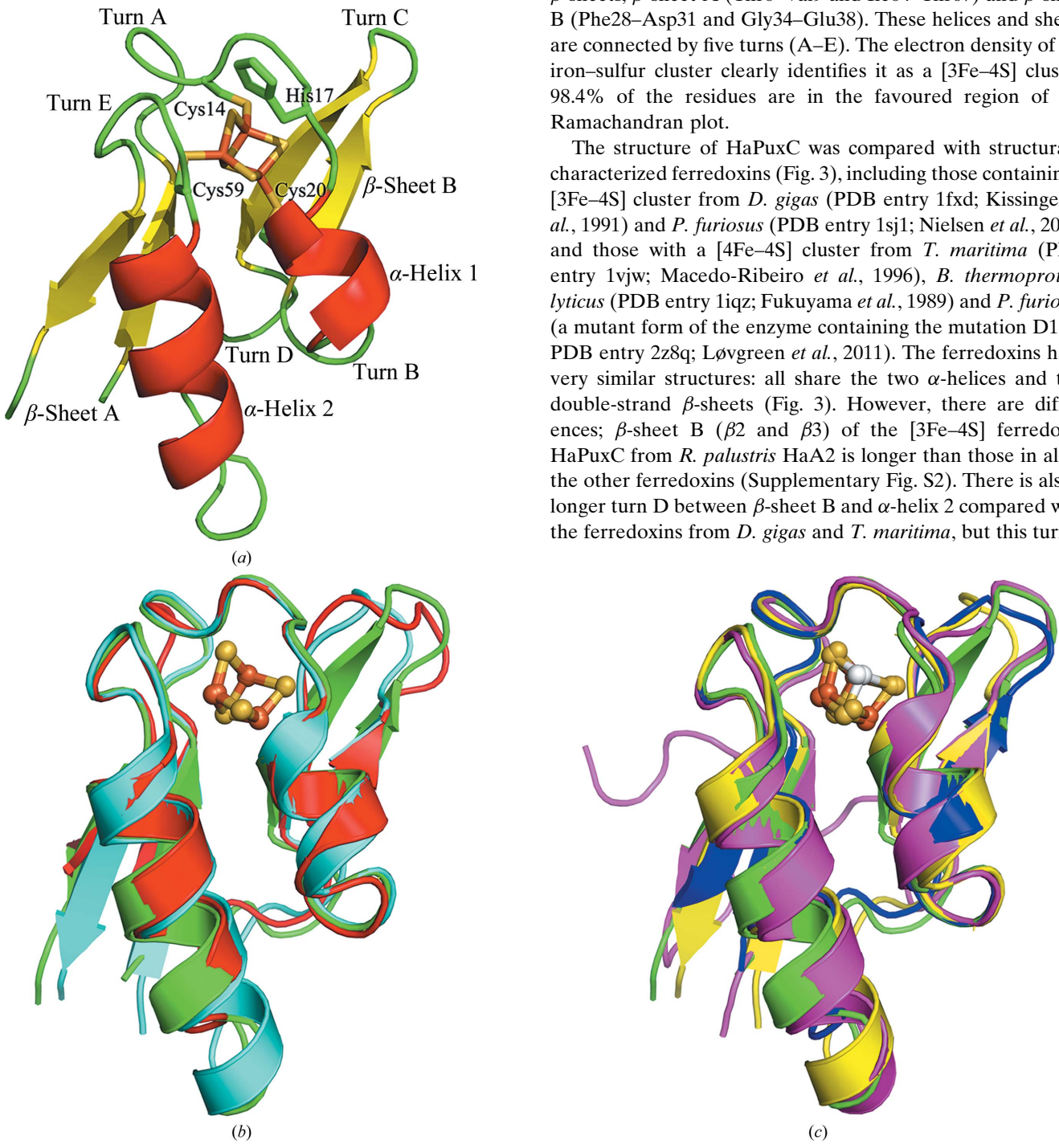

Figure 3
(*a*) The overall structure of the ferredoxin HaPuxC from *R. palustris* HaA2. α-Helices 1 and 2, β-sheets A and B, and turns A–E are shown in red, yellow and green, respectively. Cys14, Cys20, Cys59, His17 and the [3Fe–4S] cluster are highlighted (sulfide ions and cysteine sulfurs in gold and iron ions in orange). (*b*, *c*) Structural comparison of the [3Fe–4S] ferredoxin RPB3630 from *R. palustris* HaA2 with other structurally characterized [3Fe–4S] and [4Fe–4S] ferredoxins. HaPuxC (green) is superimposed with (*b*) the [3Fe–4S] ferredoxins from *D. gigas* (PDB entry 1fxd; red) and *P. furiosus* (PDB entry 1sj1; cyan) and (*c*) the [4Fe–4S] ferredoxins from *B. thermoproteolyticus* (PDB entry 1iqz; magenta), *T. maritima* (PDB entry 1vjw; blue) and *P. furiosus* (PDB entry 2z8q; yellow). The Fe–S clusters are shown in ball-and-stick format (Fe, orange; S, gold); a white sphere is used to designate the position of the fourth Fe atom in [4Fe–4S] clusters in (*c*).

shorter than the equivalent in the ferredoxin from *B. thermoproteolyticus*. Analysis of the primary sequence highlights differences in this region which account for these observations (Fig. 2). α-Helix 2 of the ferredoxins from *B. thermoproteolyticus* and *P. furiosus* are longer than those from *R. palustris* HaA2, *T. maritima* and *D. gigas*, which are of a similar length. The extension of this helix occurs at the N-terminus (the end closest to the D turn). In addition to having a longer turn D, the ferredoxin from *B. thermoproteolyticus* (PDB entry 1iqz) has a longer C-terminal loop.

Comparison of the orientation of turn A relative to the iron–sulfur cluster revealed differences between the [3Fe–4S] cluster and the [4Fe–4S] cluster ferredoxins. In the [3Fe–4S] cluster ferredoxins this loop bends towards the vacant site of the cluster by 1.1–1.2 Å. The bending of this loop occurs at the residue corresponding to His17 of *R. palustris* HaA2 (Asp14 in the case of *P. furiosus*) or the fourth cluster-binding cysteine in the [4Fe–4S] ferredoxins (Fig. 3 and Supplementary Fig. S3).

The ferredoxins from the thermophilic bacteria *T. litoralis*, *C. thermoaceticum* and *P. furiosus* contain an additional pair of cysteine residues (Cys21 and Cys48 in *P. furiosus*) which form a disulfide bond in either a right-handed or left-handed spiral configuration (Macedo-Ribeiro *et al.*, 1996; Nielsen *et al.*, 2004; Løvgreen *et al.*, 2011). This disulfide bond has been shown to play a role in the redox cycling of these ferredoxins (Gorst *et al.*, 1995). This pair of cysteine residues is absent in the other ferredoxins, including those from *R. palustris* strains, although *saro_3681* from *N. aromaticivorans* contains one cysteine residue at the position equivalent to Cys21.

3.4. Cluster environment

In the structure of HaPuxC the electron-density map of the Fe–S cluster clearly shows that it is a complete [3Fe–4S] cluster and that there are no water molecules located nearby. The cluster is coordinated by Fe—S^{γ} bonds to cysteines 14, 20 and 59 (Fig. 4). The geometries of the [3Fe–4S] cluster are similar to those observed for other clusters of this type, and the bond lengths between the cysteinyl sulfur and Fe are in the range of normal Fe–S proteins: from 2.2 to 2.3 Å (Fig. 4). Turn A at His17 moves towards to the vacant site of the [3Fe–4S] cofactor and consequently the C^{β} of His17 is closer to the cluster. However, the side chain of His17 is turned away from the cluster and both N atoms of the imidazole ring interact with the $O^{\varepsilon 1}$ atom of Glu61 (3.4 and 3.5 Å; Fig. 4). $N^{\delta 1}$ also hydrogen bonds to S2 of the [3Fe–4S] cluster (distance of 3.6 Å). Thus, while histidine is located close to where a fourth iron would be positioned in a [4Fe-4S] cluster, its side chain points towards the exterior of the protein (Figs. 3, 4 and Supplementary Fig. S3). The Glu61 residue of HaPuxC, which

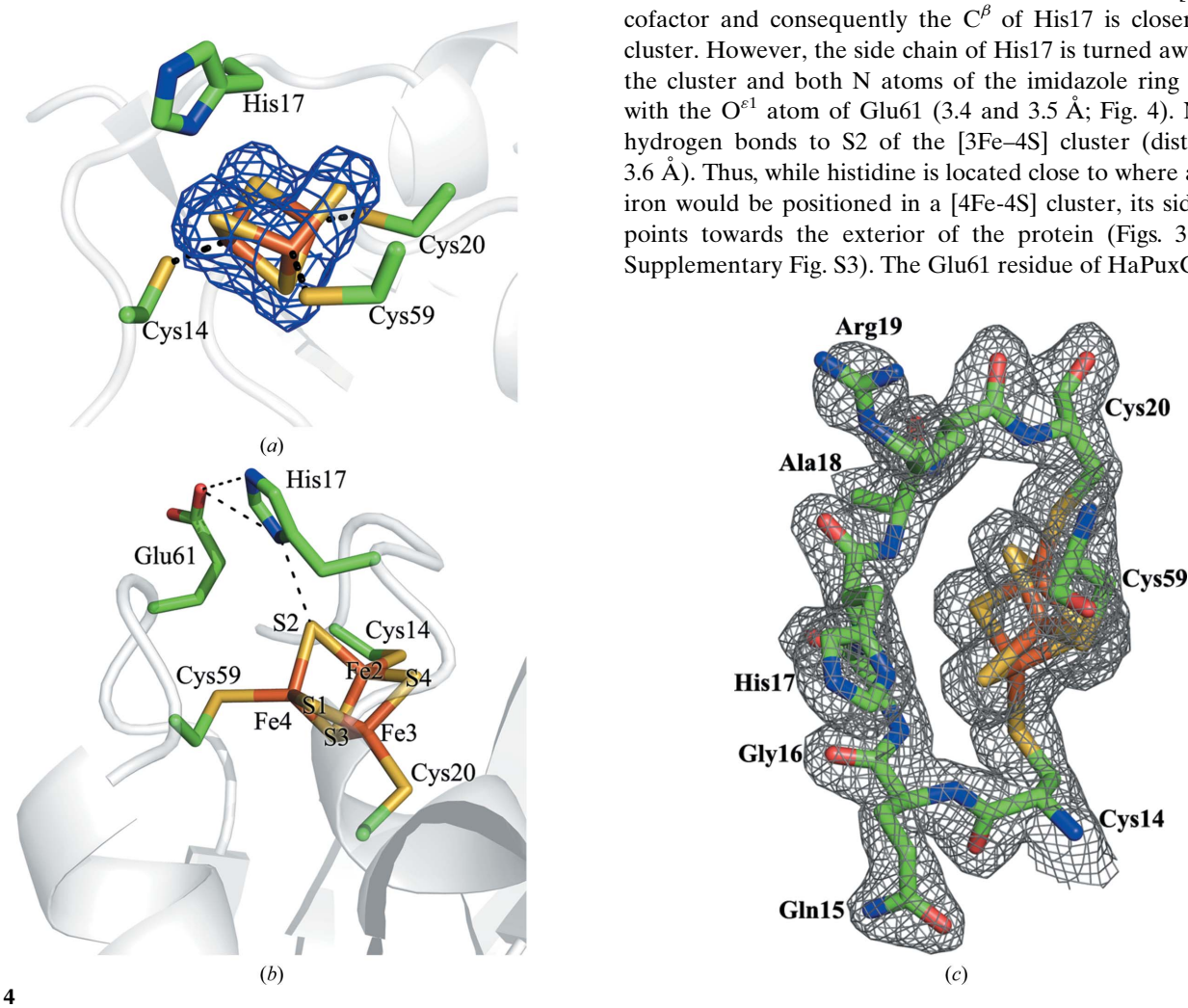

Figure 4
(*a*) The [3Fe–4S] cluster of the ferrodoxin HaPuxC and the surrounding residues (residues in green; Fe, orange; S, gold; N, blue). The $2mF_o - DF_c$ density of the cluster and His17 are shown contoured at ∼0.35 e Å^{-3} (blue mesh). (*b*) Cluster environment of HaPuxC (green). (*c*) The iron–sulfur cluster environment of HaPuxC with residues that interact with the cluster. (Fe, orange, S; gold, C; green; N, blue, O, red; Supplementary Table S1). The $2mF_o - DF_c$ density of the cluster and the residues are shown contoured at ∼0.35 e Å^{-3} (grey mesh).

hydrogen bonds to His17, is conserved among the histidine-containing ferredoxins from *R. palustris*, *B. japonicum* and *N. aromaticivorans* but not those from the *Mycobacterium* species (Fig. 2).

With the exception of the empty cubane cluster site close to His17, the cluster is shielded from direct solvent contact by the backbone of residues 14–20 and by the side chains of Val9, Gln15, Ala18, Arg19, Phe28, Glu61 and Ala63 (Fig. 4*c*; Nielsen *et al.*, 2004). Sulfurs S1, S2 and S4 of the cluster and the S^{γ} atoms of the cysteines participate in an NH···S hydrogen-bonding network that stabilizes the cluster and the structure (Table 2, Fig. 5). Such a hydrogen-bonding network is also observed in other structurally characterized ferredoxins (Fukuyama *et al.*, 1989; Nielsen *et al.*, 2004), although it appears to be more extensive in HaPuxC (Table 2 and Fig. 5).

3.5. The interaction face of HaPuxC

The electrostatic surface potential of HaPuxC from *R. palustris* HaA2 (Fig. 6) indicates that the likely interaction face of the ferredoxin surrounding the iron–sulfur cluster region is predominantly negatively charged. There are five acidic amino-acid residues, Asp12, Asp50, Glu61, Glu68 and Asp69, and one positively charged residue, Arg19, on the surface. Glu61 resides in one of the cluster-binding loops, resulting in the area above the cluster being negatively charged. A comparison with the surfaces of the [4Fe–4S] ferredoxin from *B. thermoproteolyticus* (PDB entry 1iqz) and the [3F–4S] form of the *P. furiosus* ferredoxin (PDB entry 1sj1) reveals that several of these residues are conserved, maintaining an overall negatively charged surface (Fig. 6). However, the surface of the cluster-binding loops in HaPuxC is more negative when compared with the other ferredoxins. As noted previously, Glu61 is conserved among the histidine-containing ferredoxins from *R. palustris*, *B. japonicum* and *N. aromaticivorans*, and this residue may be important in the ferredoxin–CYP interaction.

A structural model of the [3Fe–4S] ferredoxin from *M. tuberculosis* (the product of gene *Rv0763c*) was generated using the *SWISS-MODE*L homology-modelling server (http://swissmodel.expasy.org/). The electrostatic surface potential of this protein was less negatively charged, with only two of the five acidic residues being conserved. The negative charge on the surface of these ferredoxins suggests that the proximal

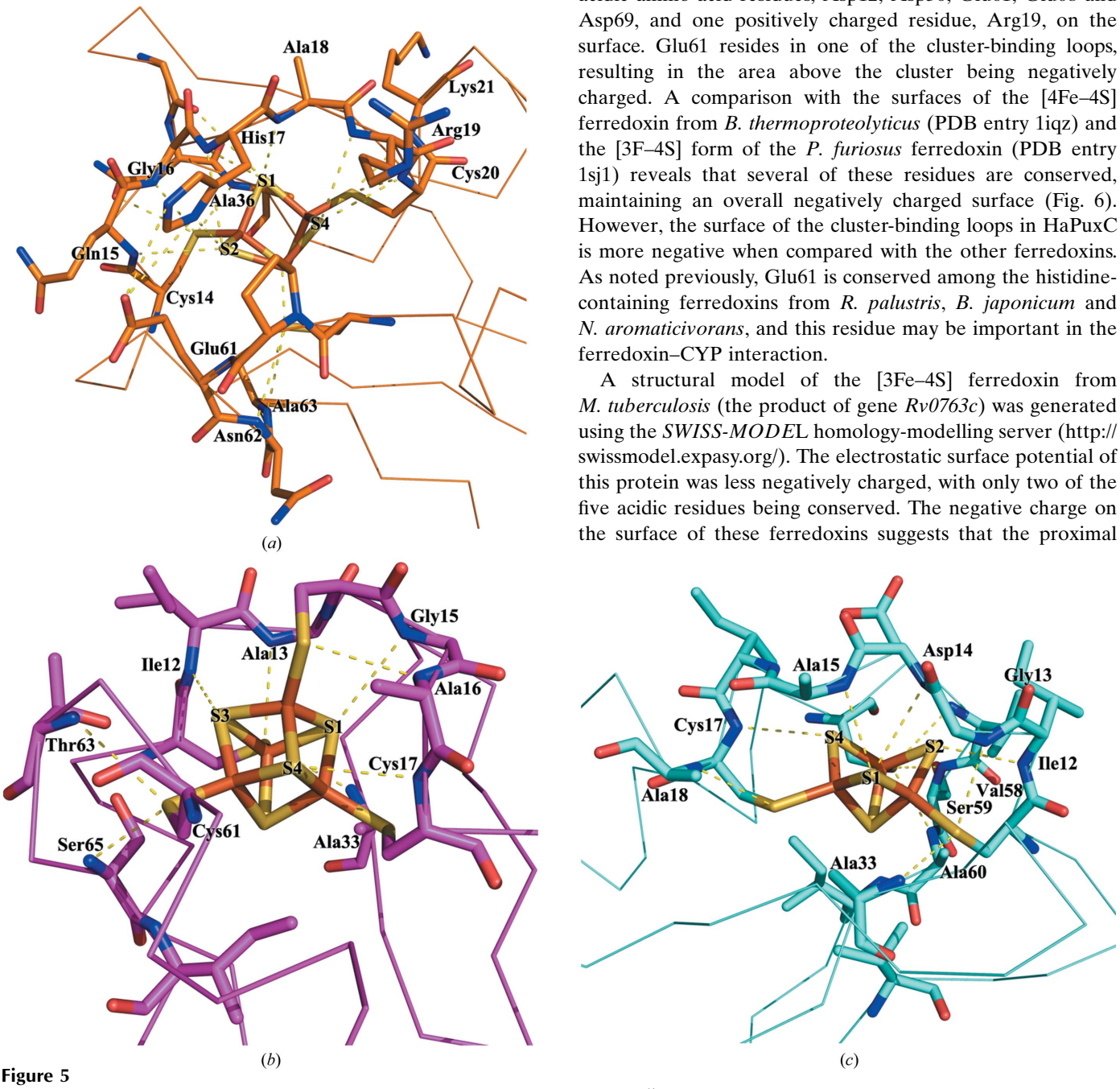

Figure 5
1The NH···S hydrogen-bonding network between S1, S2 and S4 of the cluster and the S^{γ} atoms of the cysteines and the backbone amide N atoms which stabilizes the cluster of (*a*) HaPuxC (orange), (*b*) the [4Fe–4S] cluster ferredoxin from *B. thermoproteolyticus* (magenta) and (*c*) the [3Fe–4S] cluster from of the ferredoxin from *P. furiosus* (cyan). The Fe–S clusters are shown in orange (Fe) and gold (S) and hydrogen bonds are shown as yellow dashed lines (Table 2).

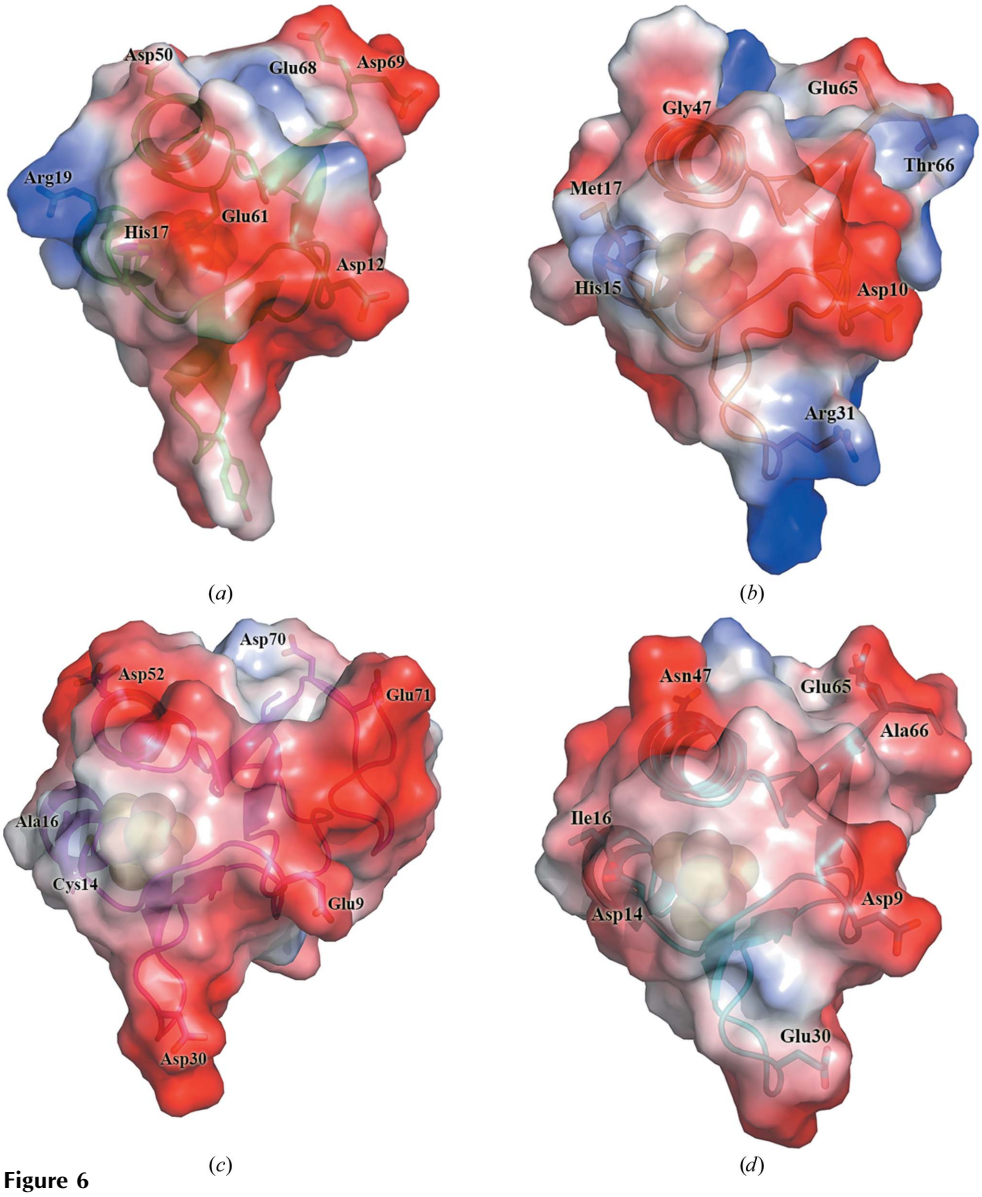

Figure 6
The electrostatic surface potentials of the interaction faces of different ferredoxins. The interaction face is defined as the region surrounding the [3Fe–4S] or [4Fe–4S] cluster regions. HaPuxC (*a*) is compared with (*b*) a model of the ferredoxin from *M. tuberculosis* (the product of gene *Rv0763c*), (*c*) oxidized [4Fe–4S] ferredoxin from *B. thermoproteolyticus* (PDB entry 1iqz) and (*d*) the [3Fe–4S] ferredoxin from the hyperthermophilic archaeon *P. furiosus* (PDB entry 1sj1). Negatively and positively charged surface areas are coloured red and blue, respectively. The electrostatic potential surface of the cluster-binding loop in HaPuxC is more negative compared with the other ferredoxins, predominantly owing to the presence of Glu61. Residues that contribute to the different surface potential distributions and that may be involved in protein recognition are labelled.

face of the equivalent CYP enzymes or other electron-transfer partners is likely to be positively charged. This is a common feature of bacterial and mitochondrial P450 enzymes which utilize ferredoxin electron-transfer partners (Supplementary Fig. S4; Bell *et al.*, 2008; Bell, Yang *et al.*, 2012; Yang *et al.*, 2010; Annalora *et al.*, 2010).

4. Discussion

Class I P450 electron-transfer systems containing [2Fe–2S] ferredoxins have been well characterized (Ewen *et al.*, 2011; Sevrioukova & Poulos, 2011; Yang *et al.*, 2010; Bell, McMillan *et al.*, 2012). Recent investigations have provided further insight into [3Fe–4S] ferredoxin- and flavodoxin-containing class I systems and fused systems (Chun *et al.*, 2007; Hawkes *et al.*, 2010; Hunter *et al.*, 2005; Whitehouse *et al.*, 2012). However, there are still many ferredoxin electron-transfer systems for which there is a lack of biochemical data, particularly structural details. The [3Fe–4S] ferredoxin from *R. palustris* HaA2 studied here has a **C***XX***H***XX***C**$(X)_n$**CP** motif rather than the usual **C***XX***C***XX***C**$(X)_n$**CP** motif of a [4Fe–4S] protein or the **C***XX***A**/**G***XX***C**$(X)_n$**CP** motif of [3Fe–4S] ferredoxins. All of the ferredoxins of this type that have been studied to date have been isolated as [3Fe–4S] ferredoxins (McLean *et al.*, 2006; Poupin *et al.*, 1999; Sielaff *et al.*, 2001) and the best characterized example is the ferredoxin (the product of gene *Rv0763c*) associated with CYP51 of *M. tuberculosis* (McLean *et al.*, 2006). The redox potential of this ferredoxin has been measured and found to be high (–31 mV), and is likely to contribute to a thermodynamic barrier to electron transfer between this electron-transfer protein and the associated CYP51 enzyme (McLean *et al.*, 2006).

Certain [2Fe–2S] ferredoxins have their iron centres coordinated by histidine residues instead of cysteines. For example, Rieske proteins have two histidine and two cysteine ligands and several [2Fe–2S] ferredoxin variants with a single histidine substitution, such as human mitoNEET9 and the yeast iron-regulatory proteins Grx3/4 and Fra2, are also known (Dicus *et al.*, 2010; Li *et al.*, 2009; Carrell *et al.*, 1997; Colbert *et al.*, 2000; Iwata *et al.*, 1996). It is significant that Rieske proteins have higher midpoint potentials compared with [2Fe–2S] ferredoxins with exclusively cysteinyl ligation (Brown *et al.*, 2008). Histidine coordination to [4Fe–4S] iron–sulfur clusters has been observed in Ni–Fe hydrogenases from *D. gigas* and *D. fructosovorans* and the Fe-only hydrogenase from *Clostridium pasteurianum* (Peters *et al.*, 1998; Volbeda *et al.*, 1995;

Table 2
NH···S interactions in the cluster of the *R. palustris* HaA2 ferredoxin HaPuxC and comparison with the interactions present in the [4Fe–4S] ferredoxin from *B. thermoproteolyticus* and the [3Fe–4S] form of the ferredoxin from *P. furiosus* (distances in Å).

R. palustris HaA2 [3Fe–4S] ferredoxin†			*B. thermoproteolyticus* [4Fe–4S] ferredoxin			*P. furiosus* [3Fe–4S] ferredoxin		
N (Gln15)	S2 (Fe–S)	3.3	N (Ile12)	S2 (Fe–S)	3.8	N (Ile12)	S2 (Fe–S)	3.3
N (Gly16)	S^{γ} (Cys14)	3.6	N (Ala13)	S^{γ} (Cys11)	3.5	N (Gly13)	S^{γ} (Cys11)	3.4
N (His17)	S2 (Fe–S)	3.7	N (Gly15)	S1 (Fe–S)	3.4	N (Asp14)	S1 (Fe–S)	3.6
N (His17)	S1 (Fe–S)	3.6	N (Ala16)	S^{γ} (Cys14)	3.6	N (Ala15)	S1 (Fe–S)	3.2
ND1 (His17)	S2 (Fe–S)	3.6	N (Cys17)	S4 (Fe–S)	3.4	N (Cys17)	S4 (Fe–S)	3.6
N (Ala18)	S1 (Fe–S)	3.2	N (Ala33)	S^{γ} (Cys11)	3.7	N (Ala18)	S^{γ} (Cys17)	3.2
N (Arg19)	S4 (Fe–S)	3.4	N (Thr63)	S^{γ} (Cys61)	3.8	N (Ala33)	S^{γ} (Cys11)	3.4
N (Cys20)	S4 (Fe–S)	3.4	N (Ser65)	S^{γ} (Cys61)	3.1	N (Val58)	S^{γ} (Cys56)†	3.7
N (Lys21)	S^{γ} (Cys20)	3.0				N (Ser59)	S^{γ} (Cys56)†	3.6
N (Als36)	S^{γ} (Cys14)	3.7				N (Ala60)	S^{γ} (Cys56)	3.4
N (Glu61)	S^{γ} (Cys59)	3.5						
N (Asn62)	S^{γ} (Cys59)	3.6						
N (Ala63)	S^{γ} (Cys59)	3.6						

† The side-chain O atom of Asn35 may interact with S (Cys14) (3.8 Å) and the N atom of the conserved proline residue Pro60 is 3.5 Å from S (Cys59).

Dementin *et al.*, 2006). Replacement of the histidine residue in the *D. fructosovorans* Ni–Fe hydrogenase impairs intermolecular and intramolecular electron transfer (Dementin *et al.*, 2006). On the other hand, mutation of the histidine coordinated to the [4Fe–4S] cluster in the Fe-only hydrogenase from *C. pasteurianum* has been reported to not significantly alter the redox potential (Adams, 1987).

Other types of ferredoxins with a noncysteinyl residue in their iron–sulfur cluster-binding motif include the aspartate-containing [3Fe–4S] ferredoxin from the thermophile *P. furiosus* (Calzolai *et al.*, 1995; Conover *et al.*, 1990; Duderstadt *et al.*, 1999; Zhou & Adams, 1997). Here, the aspartate residue is known to affect the stability and redox potential of the cluster. Aspartate and glutamate residues have also been found to coordinate to [4Fe–4S] clusters in more complex proteins such as the transcriptional regulator Fnr from *B. subtilis* and the isoprenoid-biosynthesis enzyme IspG from *Aquifex aeolicus* (Gruner *et al.*, 2011; Lee *et al.*, 2010; Løvgreen *et al.*, 2011).

There are similar histidine-containing ferredoxins to HaPuxC from *R. palustris* HaA2 in *R. palustris* strains CGA009 and BisB5 and *B. japonicum* USDA110, and these are all associated with CYP194A enzymes. The lowest sequence identity among these CYP enzymes is 75%, suggesting that the combination of a CYP194 family enzyme and a ferredoxin containing a histidine residue has been conserved across these species. Genes encoding CYP194A subfamily enzymes are also found in bacteria such as strains of *Nitrobacter* (72% sequence identity) but are not associated with a ferredoxin gene (although a similar ferredoxin is present elsewhere in the genome). Other members of the CYP194 family are found in many other bacteria such as *Pseudomonas*, *Arthrobacter* and *Ralstonia* species, but these have a much lower sequence identity when compared with the CYP194A2 and A3 enzymes (<52%).

In summary, we have determined the crystal structure of a ferredoxin containing a [3Fe–4S] cluster. A histidine ligand makes up the potential coordination sphere but is not ligated to the cluster. A detailed understanding of the role of the histidine residue, the iron–sulfur cluster and the ferredoxin as well as the function of the CYP194A subfamily of CYP enzymes will be of significant interest.

References

Adams, M. W. W. (1987). *J. Biol. Chem.* **262**, 15054–15061.
Adams, P. D. *et al.* (2010). *Acta Cryst.* D**66**, 213–221.
Annalora, A. J., Goodin, D. B., Hong, W.-X., Zhang, Q., Johnson, E. F. & Stout, C. D. (2010). *J. Mol. Biol.* **396**, 441–451.
Arnold, K., Bordoli, L., Kopp, J. & Schwede, T. (2006). *Bioinformatics*, **22**, 195–201.
Bell, S. G., French, L., Rees, N. H., Cheng, S. S., Preston, G. & Wong, L.-L. (2013). *Biotechnol. Appl. Biochem.* **60**, 9–17.
Bell, S. G., Hoskins, N., Xu, F., Caprotti, D., Rao, Z. & Wong, L.-L. (2006). *Biochem. Biophys. Res. Commun.* **342**, 191–196.
Bell, S. G., McMillan, J. H. C., Yorke, J. A., Kavanagh, E., Johnson, E. O. D. & Wong, L.-L. (2012). *Chem. Commun.* **48**, 11692.
Bell, S. G., Tan, A. B. H., Johnson, E. O. D. & Wong, L.-L. (2010). *Mol. Biosyst.* **6**, 206–214.
Bell, S. G. & Wong, L.-L. (2007). *Biochem. Biophys. Res. Commun.* **360**, 666–672.
Bell, S. G., Xu, F., Forward, I., Bartlam, M., Rao, Z. & Wong, L.-L. (2008). *J. Mol. Biol.* **383**, 561–574.
Bell, S. G., Xu, F., Johnson, E. O., Forward, I. M., Bartlam, M., Rao, Z. & Wong, L.-L. (2010). *J. Biol. Inorg. Chem.* **15**, 315–328.
Bell, S. G., Yang, W., Tan, A. B., Zhou, R., Johnson, E. O. D., Zhang, A., Zhou, W., Rao, Z. & Wong, L. L. (2012). *Dalton Trans.* **41**, 8703–8714.
Bell, S. G., Zhou, R., Yang, W., Tan, A. B., Gentleman, A. S., Wong, L.-L. & Zhou, W. (2012). *Chemistry*, **18**, 16677–16688.
Brazeau, B. J., Wallar, B. J. & Lipscomb, J. D. (2003). *Biochem. Biophys. Res. Commun.* **312**, 143–148.
Brown, E. N., Friemann, R., Karlsson, A., Parales, J. V., Couture, M. M., Eltis, L. D. & Ramaswamy, S. (2008). *J. Biol. Inorg. Chem.* **13**, 1301–1313.
Calzolai, L., Gorst, C. M., Zhao, Z. H., Teng, Q., Adams, M. W. W. & La Mar, G. N. (1995). *Biochemistry*, **34**, 11373–11384.
Capyk, J. K., Kalscheuer, R., Stewart, G. R., Liu, J., Kwon, H., Zhao, R., Okamoto, S., Jacobs, W. R. Jr, Eltis, L. D. & Mohn, W. W. (2009). *J. Biol. Chem.* **284**, 35534–35542.
Carrell, C. J., Zhang, H., Cramer, W. A. & Smith, J. L. (1997). *Structure*, **5**, 1613–1625.
Chenna, R., Sugawara, H., Koike, T., Lopez, R., Gibson, T. J., Higgins, D. G. & Thompson, J. D. (2003). *Nucleic Acids Res.* **31**, 3497–3500.

Chen, V. B., Arendall, W. B., Headd, J. J., Keedy, D. A., Immormino, R. M., Kapral, G. J., Murray, L. W., Richardson, J. S. & Richardson, D. C. (2010). *Acta Cryst.* D**66**, 12–21.
Chiu, H.-T., Hubbard, B. K., Shah, A. N., Eide, J., Fredenburg, R. A., Walsh, C. T. & Khosla, C. (2001). *Proc. Natl Acad. Sci. USA*, **98**, 8548–8553.
Chun, Y.-J., Shimada, T., Sanchez-Ponce, R., Martin, M. V., Lei, L., Zhao, B., Kelly, S. L., Waterman, M. R., Lamb, D. C. & Guengerich, F. P. (2007). *J. Biol. Chem.* **282**, 17486–17500.
Colbert, C. L., Couture, M. M., Eltis, L. D. & Bolin, J. T. (2000). *Structure*, **8**, 1267–1278.
Conover, R. C., Kowal, A. T., Fu, W., Park, J.-B., Aono, S., Adams, M. W. W. & Johnson, M. K. (1990). *J. Biol. Chem.* **265**, 8533–8541.
Cordes, M. & Giese, B. (2009). *Chem. Soc. Rev.* **38**, 892–901.
Dementin, S., Belle, V., Bertrand, P., Guigliarelli, B., Adryanczyk-Perrier, G., De Lacey, A. L., Fernandez, V. M., Rousset, M. & Léger, C. (2006). *J. Am. Chem. Soc.* **128**, 5209–5218.
Dicus, M. M., Conlan, A., Nechushtai, R., Jennings, P. A., Paddock, M. L., Britt, R. D. & Stoll, S. (2010). *J. Am. Chem. Soc.* **132**, 2037–2049.
Duderstadt, R. E., Staples, C. R., Brereton, P. S., Adams, M. W. W. & Johnson, M. K. (1999). *Biochemistry*, **38**, 10585–10593.
Elliott, J. I., Yang, S. S., Ljungdahl, L. G., Travis, J. & Reilly, C. F. (1982). *Biochemistry*, **21**, 3294–3298.
Emsley, P. & Cowtan, K. (2004). *Acta Cryst.* D**60**, 2126–2132.
Ewen, K. M., Kleser, M. & Bernhardt, R. (2011). *Biochim. Biophys. Acta*, **1814**, 111–125.
Fukuyama, K., Matsubara, H., Tsukihara, T. & Katsube, Y. (1989). *J. Mol. Biol.* **210**, 383–398.
Gorst, C. M., Zhou, Z. H., Ma, K., Teng, Q., Howard, J. B., Adams, M. W. W. & La Mar, G. N. (1995). *Biochemistry*, **34**, 8788–8795.
Gouet, P., Robert, X. & Courcelle, E. (2003). *Nucleic Acids Res.* **31**, 3320–3323.
Green, A. J., Munro, A. W., Cheesman, M. R., Reid, G. A., von Wachenfeldt, C. & Chapman, S. K. (2003). *J. Inorg. Biochem.* **93**, 92–99.
Gruner, I., Frädrich, C., Böttger, L. H., Trautwein, A. X., Jahn, D. & Härtig, E. (2011). *J. Biol. Chem.* **286**, 2017–2021.
Hannemann, F., Bichet, A., Ewen, K. M. & Bernhardt, R. (2007). *Biochim. Biophys. Acta*, **1770**, 330–344.
Hawkes, D. B., Adams, G. W., Burlingame, A. L., Ortiz de Montellano, P. R. & De Voss, J. J. (2002). *J. Biol. Chem.* **277**, 27725–27732.
Hawkes, D. B., Slessor, K. E., Bernhardt, P. V. & De Voss, J. J. (2010). *Chembiochem*, **11**, 1107–1114.
Hunter, D. J., Roberts, G. A., Ost, T. W., White, J. H., Müller, S., Turner, N. J., Flitsch, S. L. & Chapman, S. K. (2005). *FEBS Lett.* **579**, 2215–2220.
Iwata, S., Saynovits, M., Link, T. A. & Michel, H. (1996). *Structure*, **4**, 567–579.
Jackson, C. J., Lamb, D. C., Marczylo, T. H., Warrilow, A. G., Manning, N. J., Lowe, D. J., Kelly, D. E. & Kelly, S. L. (2002). *J. Biol. Chem.* **277**, 46959–46965.
Jackson, R. G., Rylott, E. L., Fournier, D., Hawari, J. & Bruce, N. C. (2007). *Proc. Natl Acad. Sci. USA*, **104**, 16822–16827.
Johnson, D. C., Dean, D. R., Smith, A. D. & Johnson, M. K. (2005). *Annu. Rev. Biochem.* **74**, 247–281.
Kaneko, T. *et al.* (2002). *DNA Res.* **9**, 189–197.
Kiefer, F., Arnold, K., Künzli, M., Bordoli, L. & Schwede, T. (2009). *Nucleic Acids Res.* **37**, D387–D392.
Kissinger, C. R., Sieker, L. C., Adman, E. T. & Jensen, L. H. (1991). *J. Mol. Biol.* **219**, 693–715.
Lamb, D. C., Skaug, T., Song, H.-L., Jackson, C. J., Podust, L. M., Waterman, M. R., Kell, D. B., Kelly, D. E. & Kelly, S. L. (2002). *J. Biol. Chem.* **277**, 24000–24005.
Larimer, F. W. *et al.* (2004). *Nature Biotechnol.* **22**, 55–61.
Lee, M., Gräwert, T., Quitterer, F., Rohdich, F., Eppinger, J., Eisenreich, W., Bacher, A. & Groll, M. (2010). *J. Mol. Biol.* **404**, 600–610.
Li, H., Mapolelo, D. T., Dingra, N. N., Naik, S. G., Lees, N. S., Hoffman, B. M., Riggs-Gelasco, P. J., Huynh, B. H., Johnson, M. K. & Outten, C. E. (2009). *Biochemistry*, **48**, 9569–9581.
Løvgreen, M. N., Martic, M., Windahl, M. S., Christensen, H. E. M. & Harris, P. (2011). *J. Biol. Inorg. Chem.* **16**, 763–775.
Macedo-Ribeiro, S., Darimont, B., Sterner, R. & Huber, R. (1996). *Structure*, **4**, 1291–1301.
Mandai, T., Fujiwara, S. & Imaoka, S. (2009). *FEBS J.* **276**, 2416–2429.
McCoy, A. J., Grosse-Kunstleve, R. W., Adams, P. D., Winn, M. D., Storoni, L. C. & Read, R. J. (2007). *J. Appl. Cryst.* **40**, 658–674.
McLean, K. J., Lafite, P., Levy, C., Cheesman, M. R., Mast, N., Pikuleva, I. A., Leys, D. & Munro, A. W. (2009). *J. Biol. Chem.* **284**, 35524–35533.
McLean, K. J., Warman, A. J., Seward, H. E., Marshall, K. R., Girvan, H. M., Cheesman, M. R., Waterman, M. R. & Munro, A. W. (2006). *Biochemistry*, **45**, 8427–8443.
Meyer, J. (2008). *J. Biol. Inorg. Chem.* **13**, 157–170.
Munro, A. W., Girvan, H. M. & McLean, K. J. (2007). *Nat. Prod. Rep.* **24**, 585–609.
Nelson, D. R., Koymans, L., Kamataki, T., Stegeman, J. J., Feyereisen, R., Waxman, D. J., Waterman, M. R., Gotoh, O., Coon, M. J., Estabrook, R. W., Gunsalus, I. C. & Nebert, D. W. (1996). *Pharmacogenetics*, **6**, 1–42.
Nielsen, M. S., Harris, P., Ooi, B. L. & Christensen, H. E. (2004). *Biochemistry*, **43**, 5188–5194.
Oda, Y., Larimer, F. W., Chain, P. S., Malfatti, S., Shin, M. V., Vergez, L. M., Hauser, L., Land, M. L., Braatsch, S., Beatty, J. T., Pelletier, D. A., Schaefer, A. L. & Harwood, C. S. (2008). *Proc. Natl Acad. Sci. USA*, **105**, 18543–18548.
Oda, Y., Meijer, W. G., Gibson, J. L., Gottschal, J. C. & Forney, L. J. (2004). *Microb. Ecol.* **47**, 68–79.
Oda, Y., Wanders, W., Huisman, L. A., Meijer, W. G., Gottschal, J. C. & Forney, L. J. (2002). *Appl. Environ. Microbiol.* **68**, 3467–3477.
Otwinowski, Z. & Minor, W. (2001). *International Tables for Crystallography*, Vol. *F*, edited by M. G. Rossmann & E. Arnold, pp. 226–235. Dordrecht: Kluwer Academic Publishers.
Painter, J. & Merritt, E. A. (2006*a*). *Acta Cryst.* D**62**, 439–450.
Painter, J. & Merritt, E. A. (2006*b*). *J. Appl. Cryst.* **39**, 109–111.
Peitsch, M. C. (1995). *Biotechnology*, **13**, 658–660.
Peters, J. W., Lanzilotta, W. N., Lemon, B. J. & Seefeldt, L. C. (1998). *Science*, **282**, 1853–1858.
Poupin, P., Ducrocq, V., Hallier-Soulier, S. & Truffaut, N. (1999). *J. Bacteriol.* **181**, 3419–3426.
Roberts, G. A., Grogan, G., Greter, A., Flitsch, S. L. & Turner, N. J. (2002). *J. Bacteriol.* **184**, 3898–3908.
Sambrook, J., Fritsch, E. F. & Maniatis, T. (1989). *Molecular Cloning: A Laboratory Manual*, 2nd ed. New York: Cold Spring Harbor Laboratory Press.
Sevrioukova, I. F. & Poulos, T. L. (2011). *Arch. Biochem. Biophys.* **507**, 66–74.
Sielaff, B. & Andreesen, J. R. (2005). *FEBS J.* **272**, 1148–1159.
Sielaff, B., Andreesen, J. R. & Schräder, T. (2001). *Appl. Microbiol. Biotechnol.* **56**, 458–464.
Sineva, E. V. & Davydov, D. R. (2010). *Biochemistry*, **49**, 10636–10646.
Volbeda, A., Charon, M.-H., Piras, C., Hatchikian, E. C., Frey, M. & Fontecilla-Camps, J. C. (1995). *Nature (London)*, **373**, 580–587.
Warrilow, A. G., Jackson, C. J., Parker, J. E., Marczylo, T. H., Kelly, D. E., Lamb, D. C. & Kelly, S. L. (2009). *Antimicrob. Agents Chemother.* **53**, 1157–1164.
Whitehouse, C. J., Bell, S. G. & Wong, L.-L. (2012). *Chem. Soc. Rev.* **41**, 1218–1260.

Whitehouse, C. J., Bell, S. G., Yang, W., Yorke, J. A., Blanford, C. F., Strong, A. J., Morse, E. J., Bartlam, M., Rao, Z. & Wong, L.-L. (2009). *Chembiochem*, **10**, 1654–1656.
Xu, F., Bell, S. G., Lednik, J., Insley, A., Rao, Z. & Wong, L.-L. (2005). *Angew. Chem. Int. Ed. Engl.* **44**, 4029–4032.
Xu, F., Bell, S. G., Peng, Y., Johnson, E. O., Bartlam, M., Rao, Z. & Wong, L.-L. (2009). *Proteins*, **77**, 867–880.
Yang, W., Bell, S. G., Wang, H., Zhou, W., Hoskins, N., Dale, A., Bartlam, M., Wong, L.-L. & Rao, Z. (2010). *J. Biol. Chem.* **285**, 27372–27384.
Zhou, Z. H. & Adams, M. W. W. (1997). *Biochemistry*, **36**, 10892–10900.